Supplementary table S1. Summary of number (N) of lens samples at each age for each genotype as well as number of lens samples that show functional and dysfunctional GRIN profiles. [1]Examples showing what is meant by asymmetrical, distortions, indentation and dip in the centre are given in Supplementary Figure S4.

genotype	Age (dpf)	N of lens	functional GRIN		dysfunctional GRIN		
			symmetrical smooth	asymmetrical[1]	distortions[1]	indentation[1]	dip in the centre[1]
Senile wildtype	1013	10	10	-	-	4	-
	1541	5	2	1	-	2	-
	1939	8	8	-	-	8	-
aqp0a$^{-/-}$	19	7	7	-	-	-	-
	63	4	4	-	-	-	-
	66	3	3	-	-	-	-
	143	3	3	-	-	-	-
	349	6	4	-	1	1	-
	396	8	1	3	-	4	-
	531	6	3	3	-	-	-
	676	4	-	-	3	1	-
	882	2	-	-	2	2	-
aqp0b$^{-/-}$	19	7	7	-	-	-	-
	32	8	8	-	-	-	-
	37	7	7	-	-	-	-
	63	6	6	-	-	-	-
	66	4	4	-	-	-	-
	119	9	9	-	-	-	-
	143	6	6	-	-	-	-
	390	6	6	-	-	-	-
	440	6	6	-	-	-	-
	748	8	6	-	-	2	-
	859	10	6	2	-	2	-
	1147	8	4	-	-	4	-
	1180	2	1	-	-	1	-
aqp0a$^{-/-}$/ *aqp0b*$^{-/-}$	11	2	2	-	-	-	-
	15	8	8	-	-	-	-
	126	5	1	4	-	-	-
	139	6	-	3	1	-	2
	304	6	-	-	1	-	5
	363	4	-	-	4	-	-
	403	4	-	1	3	-	-
	505	8	-	1	4	-	5
	679	6	-	-	2	1	3
	713	4	-	1	2	-	1
	727	1	-	-	1	-	-

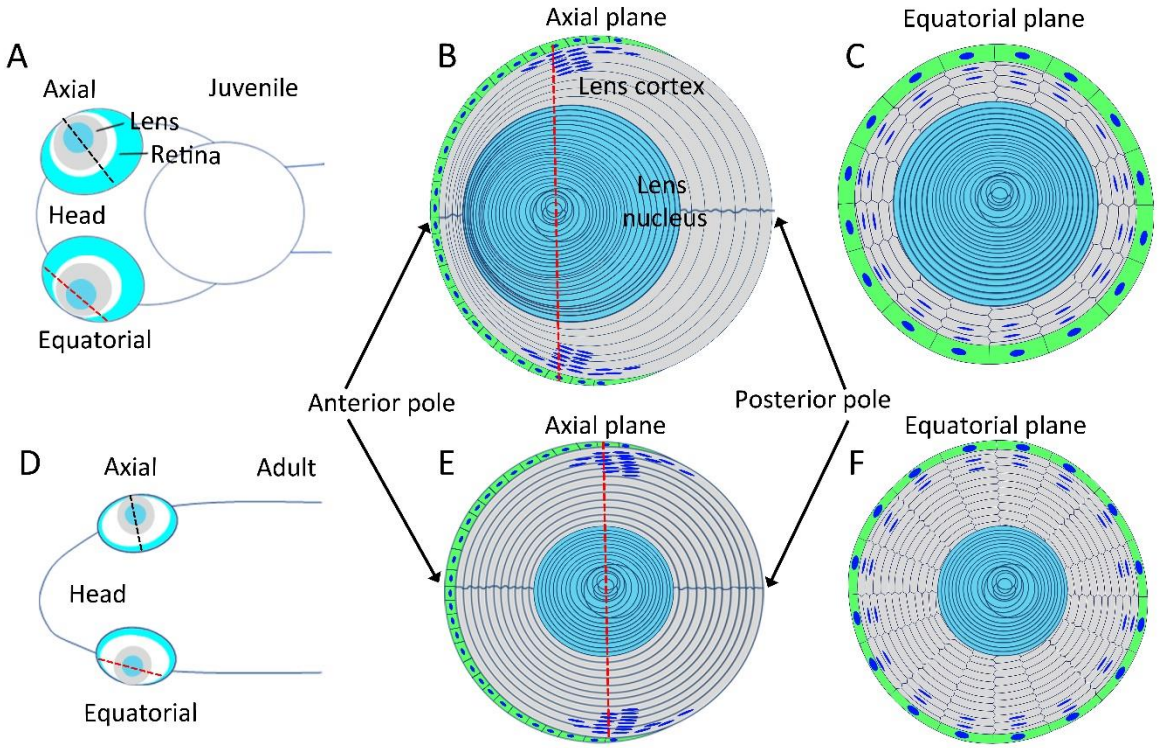

Supplementary figure S1. Orientations of lens axial and equatorial planes in juvenile and adult zebrafish. Diagrammatic view of a zebrafish juvenile (A) and adult head (D) showing the position of eyes and lenses. Lens axial plane (black dashed line) shown in higher detail (B, E) reveals relative localisation of the lens nucleus in the optical axis and allows study of the anterior and posterior poles. The equatorial lens plane passes through the centre of the lens nucleus, which is closer to the anterior pole in younger lenses (B, red dashed line), and through the centre in adult WT lenses (E, red dashed line), shown in higher detail in C, F.

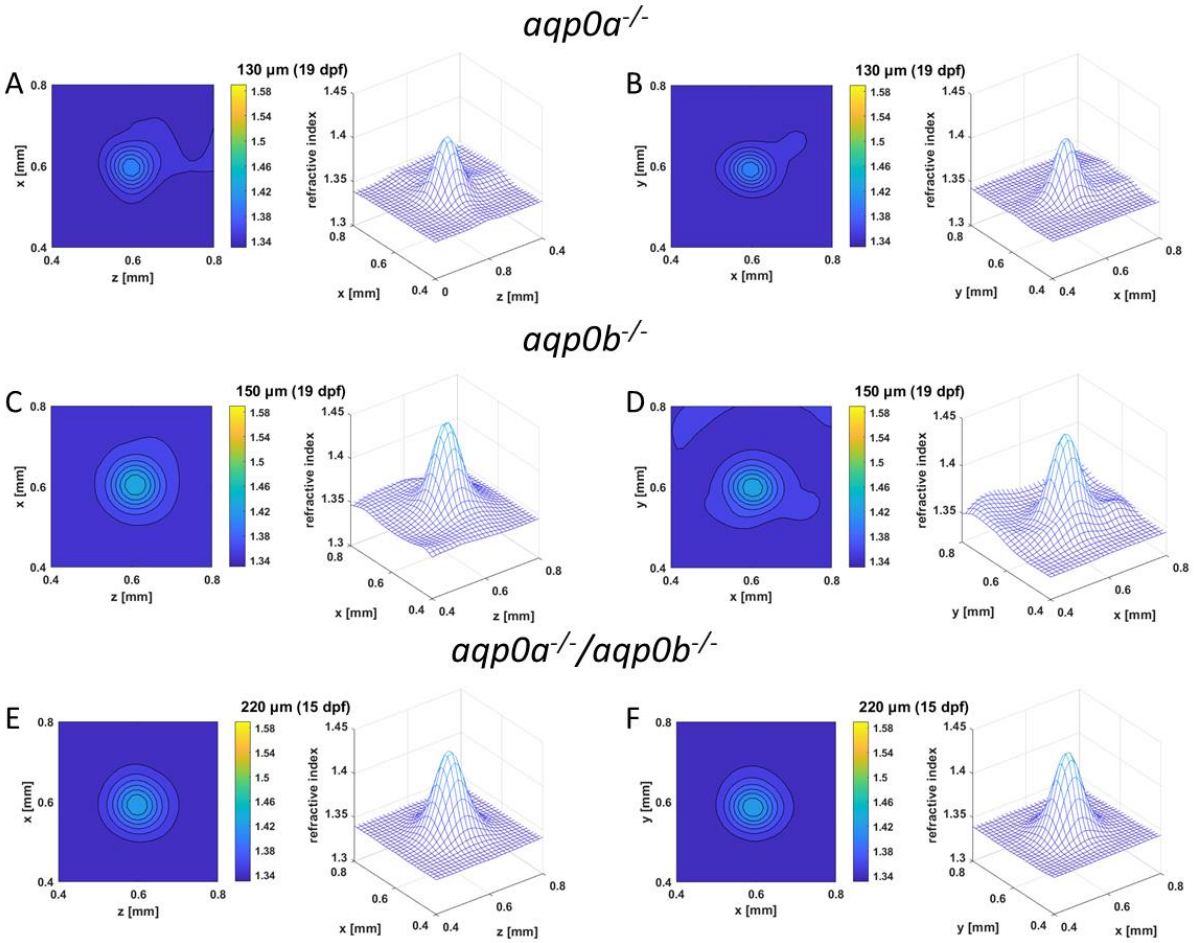

Supplementary figure S2. GRIN distributions of lenses from young larval Aqp0 mutant zebrafish. Higher magnification of the two-dimensional contour plots (left panels) and three-dimensional mesh plots (right panels) of GRIN distribution in the 0-degree plane (left column) and the 90-degree plane (right column) of (A, B) *aqp0a*$^{-/-}$ lens at 19dpf, (C, D) *aqp0b*$^{-/-}$ lens at 19dpf, and (E, F) double *aqp0a*$^{-/-}$*/ aqp0b*$^{-/-}$ mutant lens at 15dpf taken from Figure 2A-B, 3A-B, 4A-B.

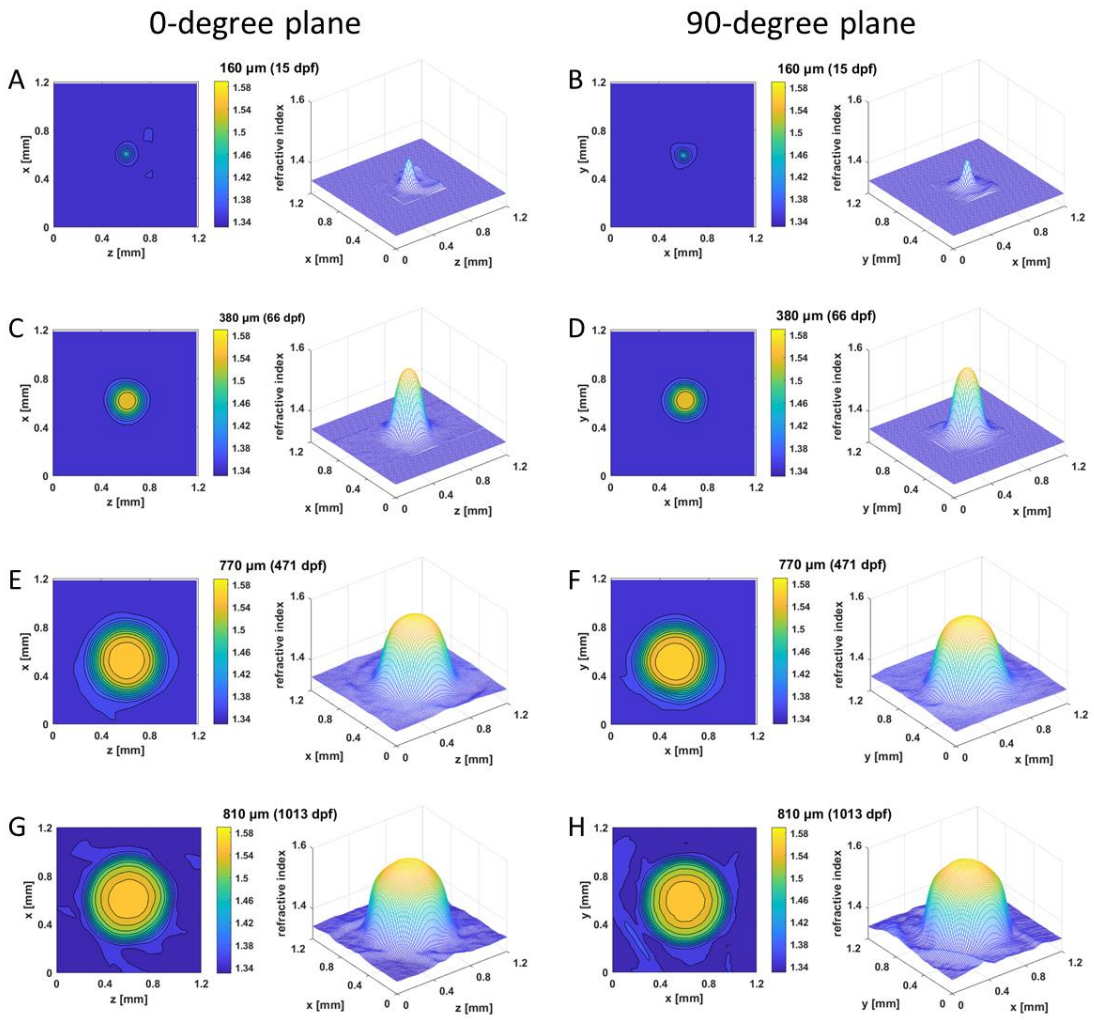

Supplementary figure S3. GRIN distributions in WT lenses. Two-dimensional contour plot (left panels) and three-dimensional mesh plot (right panels) of GRIN distribution in WT lenses in the 0°plane, representing the equatorial plane (left column) and 90° plane, representing the axial plane (right column) of four selected lenses with diameters ranging from 160 to 810 µm at specified dpf that cover an age range that is comparable with the lenses from mutant zebrafish.

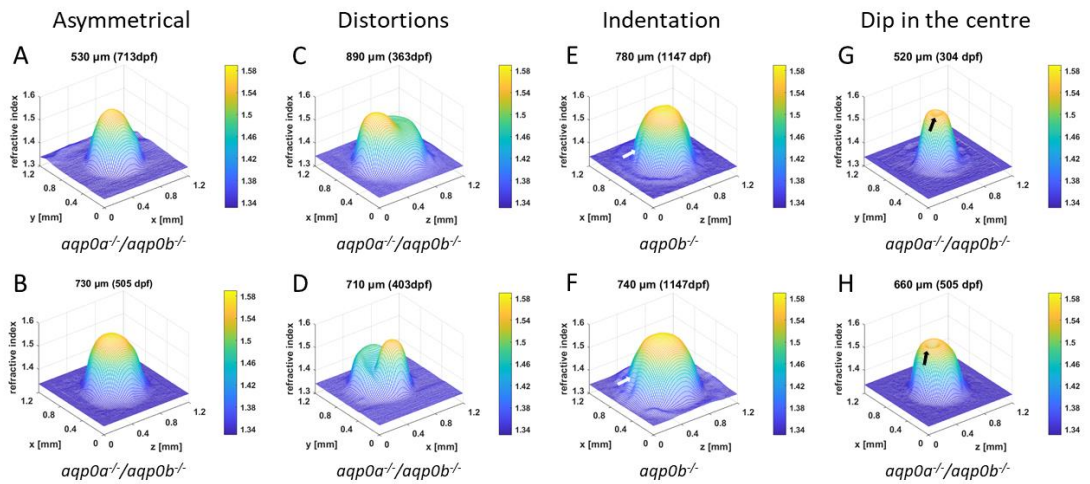

Supplementary figure S4. Types of disruptions to the GRIN profiles seen in zebrafish lenses. Examples of GRIN profiles that (A-B) are asymmetrical (asymmetrically located nucleus), (C-D) show distortions, (E-F) have indentations (marked by white arrows) and (G-H) have a dip in the centre (marked by black arrows).

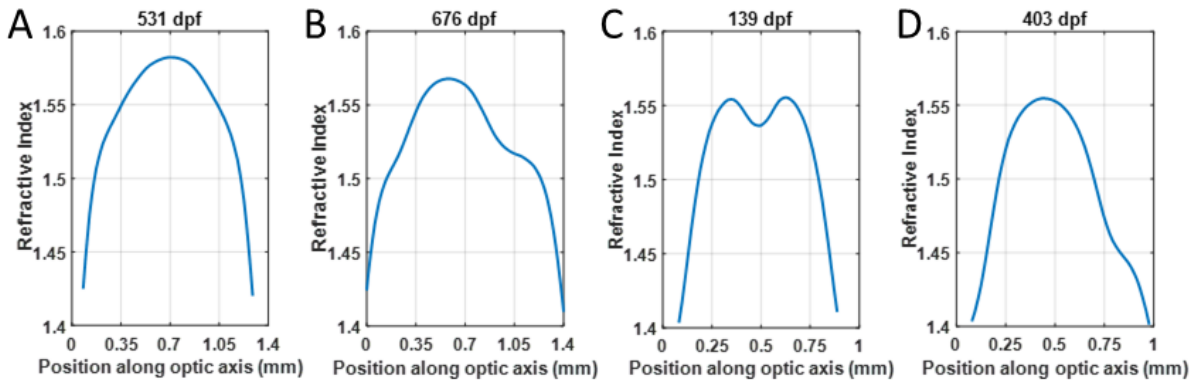

Supplementary figure S5. GRIN profiles demonstrate markedly altered shapes. GRIN profile plotted against position along optic axis for *aqp0a*$^{-/-}$ lens at 531 dpf (A) and 676 dpf (B), double *aqp0a*$^{-/-}$/ *aqp0b*$^{-/-}$ mutant lens at 139 dpf (C) and 403 dpf (D). The profiles of the mutant lenses deviate from a smooth parabolic form in different ways for the varying mutations. In all cases such deviations would impede the passage of light to the retina and detrimentally affect image quality.